

Reinforced Masonry Building Seismic Response Models for ASCE/SEI-41

Mohamed Ezzeldin, A.M.ASCE¹; Wael El-Dakhkhni, F.ASCE²; and Lydell Wiebe, A.M.ASCE³

Abstract: The development of models to predict the inelastic behavior of the individual components of a building system at different performance levels is an essential step in performing nonlinear static and dynamic analyses, as recommended by ASCE/SEI-41. However, current methodologies for generating nonlinear models for reinforced masonry shear wall (RMSW) buildings do not adequately account for various system-level aspects, such as the influence of the floor slab stiffness. Several recent studies have shown that these aspects would significantly alter the overall building response under seismic loading. In addition, although ASCE/SEI-41 defines the capacity parameters of reinforced masonry shear walls (RMSWs) with rectangular cross sections through standardized force-displacement backbone relationships, no corresponding relationships are available for RMSWs with boundary elements. Moreover, ASCE/SEI-41 does not provide the necessary hysteretic parameters required to define the cyclic behavior of any type of RMSWs under seismic loading. To address these issues, this study focuses on developing two ASCE/SEI-41 relevant models for RMSW buildings, based on the currently available provisions pertaining to their reinforced concrete (RC) counterparts. The first model is a backbone model for RMSW buildings without and with boundary elements that can be used to perform nonlinear static analyses. The experimentally validated modeling approach shows that RC parameters are applicable, but it is critical to include the out-of-plane stiffness of the floor diaphragms when evaluating the overall building response. The second model is a concentrated plasticity (spring) model in *OpenSees* used to simulate the hysteretic response of RMSW buildings with different configurations, to conduct nonlinear dynamic analyses. Finally, the developed numerical hysteretic responses are compared with experimental results in terms of the most relevant characteristics, including the initial stiffness, peak load, and stiffness and strength degradation as applicable. This study aims at presenting useful system-level response prediction tools for the nonlinear static and dynamic procedures specified by ASCE/SEI-41. DOI: 10.1061/(ASCE)ST.1943-541X.0001914. © 2017 American Society of Civil Engineers.

Author keywords: Backbone model; Hysteretic response; Nonlinear analysis; *OpenSees*; Reinforced masonry; System-level behavior; Concrete and masonry structures.

Introduction

Nonlinear analysis is a common tool in both earthquake engineering practice and research because it provides the means to determine the inelastic structural response under earthquakes, including evaluating stiffness and strength degradation, as required by modern performance-based design approaches. For this reason, nonlinear analysis plays an important role in the seismic risk assessment of new and existing buildings. For example, FEMA 440 (FEMA 2005) provides a comprehensive methodology for the use of nonlinear analysis for the seismic evaluation and retrofit of existing buildings. In addition, nonlinear analysis is being used to improve and validate design codes and standards. For example, FEMA P695 (FEMA 2009) outlines procedures to generate collapse fragility curves and assess the collapse risk of buildings, in order to assess the adequacy of seismic performance factors in current codes and

standards. Moreover, nonlinear analysis facilitates the probabilistic assessment of the seismic performance of buildings following the FEMA P58 (FEMA 2012) procedure.

Nonlinear analyses require nonlinear structural response models that are capable of predicting the inelastic behavior of the individual components of a seismic-force-resisting system (SFRS) at different performance levels. These nonlinear models are typically presented in the form of backbone relationships [for nonlinear static procedure (NSP)] or hysteretic models [for nonlinear dynamic procedure (NDP)] as specified in ASCE/SEI 41-13 (ASCE/SEI 2014). Hysteretic models simulate the component/system response under cyclic loading, while backbone models (as used in this paper) simulate the backbone curves that are developed by connecting each point of peak displacement during the first cycle of each increment of loading/deformation (ASCE/SEI 2014). Both models are generally expected to capture postpeak softening response, stiffness (as applicable), and strength degradation. In addition, hysteretic models also incorporate unloading and reloading stiffnesses, cyclic deterioration, and pinching behavior.

The studies that have been conducted to develop nonlinear models for reinforced masonry shear walls (RMSWs) can be primarily categorized by the degree of model idealization as (1) continuum finite-element models, where the nonlinear behavior of the masonry and the longitudinal and shear reinforcement that comprise the shear wall are modeled explicitly (e.g., Mojsilovic and Marti 1997; Lourenço and Rots 1997; Guinea et al. 2000; Giambanco et al. 2001; Abdellatif 2011); (2) distributed plasticity (fiber) models, where numerical integration is used through the RMSW cross section and along its length to distribute plasticity

¹Postdoctoral Fellow, Dept. of Civil Engineering, McMaster Univ., Hamilton, ON, Canada L8S 4L7 (corresponding author). E-mail: ezzeldms@mcmaster.ca

²Martini Mascarini and George Chair in Masonry Design, Dept. of Civil Engineering, McMaster Univ., Hamilton, ON, Canada L8S 4L7. E-mail: eldak@mcmaster.ca

³Assistant Professor, Dept. of Civil Engineering, McMaster Univ., Hamilton, ON, Canada L8S 4L7. E-mail: wiebel@mcmaster.ca

Note. This manuscript was submitted on November 5, 2016; approved on June 14, 2017; published online on October 25, 2017. Discussion period open until March 25, 2018; separate discussions must be submitted for individual papers. This paper is part of the *Journal of Structural Engineering*, © ASCE, ISSN 0733-9445.

(e.g., Stavridis and Shing 2010; Karapitta et al. 2011; Siyam et al. 2015; Ezzeldin et al. 2016); and (3) concentrated plasticity models, where all the nonlinear effects of the RMSWs are lumped into an inelastic spring idealized by a single-degree-of-freedom relationship (e.g., moment-rotation) (Dymiotis et al. 2001; Dolšek and Fajfar 2008; Shedid et al. 2010; Andreini et al. 2014; Marques and Lourenço 2014). Although detailed continuum finite-element and distributed plasticity models can very accurately capture behaviors such as initiation of masonry cracking and steel yielding, they are nonetheless computationally intensive (ATC 2010). As such, limited studies have been conducted to capture strength degradation due to such factors as reinforcing bar buckling (e.g., Maekawa et al. 2003; Kunnath et al. 2009; Cosenza et al. 2010; Kunnath et al. 2010; Kim and Koutromanos 2016); bond slip (e.g., Monti and Spacone 2000; Salem and Maekawa 2004; Cho and Pincheira 2006; Murcia-Delso and Benson Shing 2014); and shear failure (e.g., Waugh and Sritharan 2010). Conversely, concentrated plasticity models (e.g., Clough 1966; Giberson 1967; Takizawa 1976; Lai et al. 1984; De la Llera and Chopra 1995; Dides and De la Llera 2005) can capture strength degradation effects and they do not require the level of detailed representation that is needed for both continuum finite-element and distributed plasticity models. A comprehensive overview of the different modeling approaches can be found elsewhere (Taucer et al. 1991).

Most of the published modeling studies to date have been conducted on RMSWs at the component level (i.e., individual walls), with only a few studies focused on system-level response evaluation of RMSWs (i.e., complete buildings) (e.g., Paulay 1997; Priestley et al. 2007; Ashour and El-Dakhakhni 2016; Ezzeldin et al. 2017a). Recently, several studies argued that there are specific system-level aspects (e.g., slab's in-plane and out-of-plane stiffness) that cannot be evaluated or assessed through component-level testing. For example, the in-plane slab stiffness results in different component-level strength and displacement demands from essentially identical RMSWs (Heerema et al. 2015). In addition, Stavridis et al. (2011) and Ashour et al. (2016) both conducted experimental programs that demonstrated that slab flexural coupling was an important system-level aspect that affected the overall RMSW building performance. This performance included the building stiffness, lateral resistance capacity, and trend of stiffness degradation, which in turn would significantly alter the overall building response under seismic loading.

The nonlinear models described above have considered only walls with rectangular cross sections, whereas RMSW buildings with boundary elements are a newly proposed system within the Canadian Standards Association *Design of masonry structures* S304-14 (CSA 2014). RMSWs with boundary elements are also included in the TMS 402-13/ACI 530-13/ASCE 5-13 Masonry Standards Joint Committee code (MSJC 2013), but neither design guidance nor classifications are provided to deal with such walls as a separate SFRS. The use of boundary elements in RMSWs enhances the overall seismic performance relative to traditional RMSWs (i.e., with rectangular cross sections) because closed ties and multiple layers of vertical bars can be accommodated within the boundary elements, thus providing a confining reinforcement cage (Shedid et al. 2010; Banting and El-Dakhakhni 2012; Ezzeldin et al. 2016). The nonlinear models developed in this paper also account for RMSW buildings with boundary elements in order to facilitate the development of prescriptive design requirements, as recommended by the TMS 402-13/ACI 530-13/ASCE 5-13 (MSJC 2013).

The objective of this paper is to develop backbone and hysteretic models that can be adapted to perform the NSP and NDP, respectively, for simulating the nonlinear response of RMSW buildings

with different configurations. In this respect, an analytical backbone model is developed and validated against the backbone curves of the experimental results reported by Ashour et al. (2016) and Ezzeldin et al. (2017b). These previous experimental programs are selected because they include walls with different configurations (i.e., without and with boundary elements) with a range of aspect ratios, from 1.5 to 4.6. A summary of these experimental programs is presented in the following section. The parameters currently assigned to RMSWs in ASCE/SEI 41-13 are then assessed and new parameter values are proposed and validated. The developed backbone model is subsequently utilized to create a concentrated plasticity (spring) model in *OpenSees* to simulate the hysteretic response of RMSW buildings. Finally, the experimental and numerical hysteretic responses are compared in terms of the most relevant characteristics, including the initial stiffness, peak load, stiffness and strength deteriorations, hysteretic shape, and pinching behavior at different drift levels.

Summary of the Experimental Programs

Ashour et al. (2016) tested a one-third scaled two-story asymmetrical RMSW building (referred to as Building III hereafter) under displacement-controlled quasistatic fully reversed cyclic loading, as shown in Fig. 1(a). Building III was composed of four traditional shear walls (i.e., with rectangular cross section) aligned along the

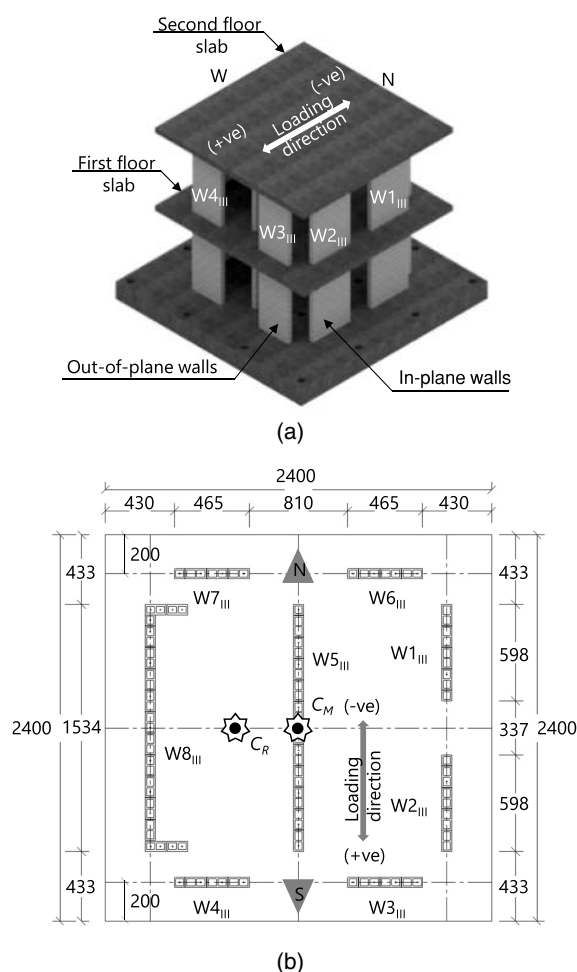


Fig. 1. Building III configuration (data from Ashour et al. 2016, © ASCE): (a) isometric view from southeast direction; (b) typical plan, all dimensions in millimeters

loading direction ($W1_{III}$, $W2_{III}$, $W5_{III}$, and $W8_{III}$) and four other walls aligned orthogonally ($W3_{III}$, $W4_{III}$, $W6_{III}$, and $W7_{III}$), as shown in Fig. 1(b). The asymmetrical wall configuration with respect to the loading direction produced an eccentricity between the building floor center of mass, C_M , and the building elastic center of rigidity, C_R , projection on the roof level. This eccentricity engaged the torsional response of the building under the applied lateral loads. The overall height of the scaled building was 2,160 mm, comprising two stories, each 1,000 mm high (corresponding to 3,000 mm at full scale), with reinforced concrete (RC) floors, each with dimensions of $2,400 \times 2,400$ mm in the plan. The building was fixed to the laboratory strong structural floor by 16 prestressed anchors through a square RC foundation ($3,000 \times 3,000$ mm).

Ezzeldin et al. (2017b) tested a similar building with the same nominal strength (to allow for a direct comparison with Building III), referred to as Building IV hereafter. The RMSWs located along the main direction of loading in Building III ($W1_{III}$, $W2_{III}$, $W5_{III}$, and $W8_{III}$) were replaced in Building IV by RMSWs with confined boundary elements ($W1_{IV}$, $W2_{IV}$, $W5_{IV}$, and $W8_{IV}$), as shown in Figs. 2(a and b). The boundary elements were adopted in Building IV because they allow closed ties to be used and multiple layers of vertical reinforced bars to be accommodated, thus providing a confining reinforcement cage, as shown in Fig. 2(c). Full details of the experimental programs can be found in papers by Ashour et al. (2016) and Ezzeldin et al. (2017b) for Buildings III and IV, respectively.

Table 1 summarizes the characteristics of the material used in Buildings III and IV reported by Ashour et al. (2016) and Ezzeldin et al. (2017b), respectively, including the masonry compressive strength of the prisms, f'_m ; the masonry Young's modulus, E_m ; the masonry shear modulus, G_m ; the yield strength of the vertical bars, f_{yv} ; and the steel reinforcement Young's modulus, E_s .

RMSW Backbone Model in ASCE/SEI 41-13

The NSP specified in ASCE/SEI 41-13 (ASCE/SEI 2014) is a more general approach for characterizing the performance of a structure than the linear procedure, which cannot be used for structures that have long periods, major setbacks, torsional or vertical stiffness irregularities, or nonorthogonal SFRS (ASCE/SEI 2014). The NSP requires analytical models that directly incorporate the non-linear load-deformation characteristics of RMSWs. These models are represented by backbone curves that include strength degradation and residual strength, if any. ASCE/SEI 41-13 (ASCE/SEI 2014) provides standardized force-displacement backbone relationships using two different approaches (referred to as Approaches 1 and 2 hereafter) for simulating the nonlinear response of RMSWs. More details regarding the definition and the assessment of these backbone curves, using Buildings III and IV, are given in this section.

Current ASCE/SEI 41-13 Backbone Modeling Approaches

In Approach 1 of ASCE/SEI 41-13 (ASCE/SEI 2014), as shown in Fig. 3, a generalized backbone curve for RMSWs is defined in terms of elastic and plastic ranges, where there is an elastic range from Point A (unloaded point) to Point B (effective yield point) and a plastic range from Point B to Point E (maximum drift point). At deformation levels greater than that corresponding to Point E, the RMSW strength is considered essentially zero. Points C and D are also defined in the plastic range of Approach 1 to represent the ultimate and residual strength points, respectively. ASCE/SEI 41-13 (ASCE/SEI 2014) defines the parameter d to represent the ultimate

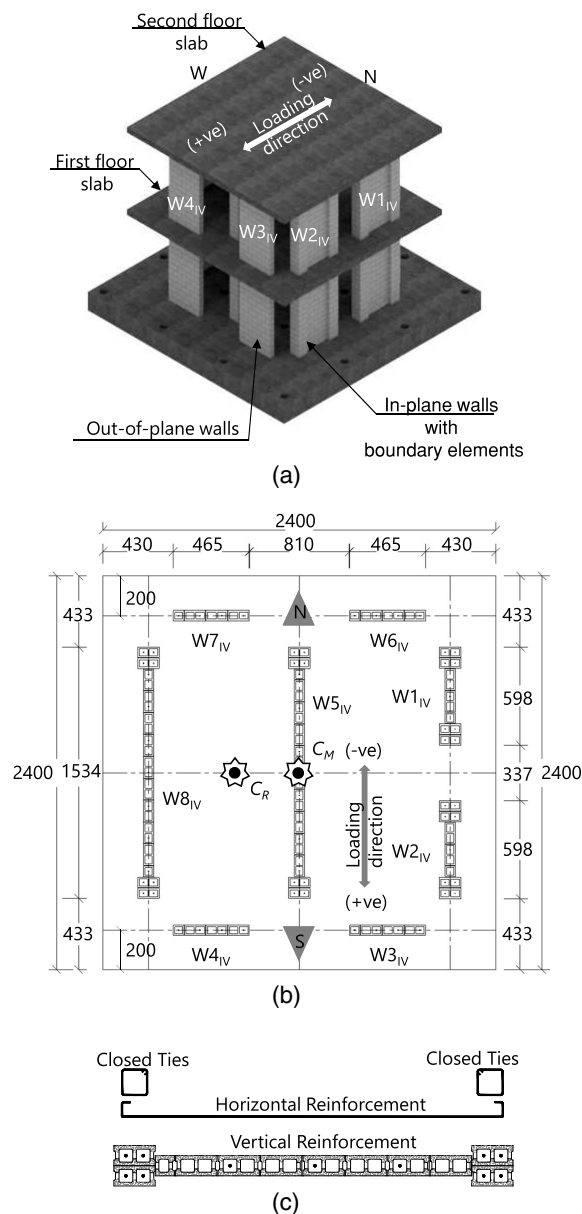


Fig. 2. Building IV configuration (data from Ezzeldin et al. 2017b, © ASCE): (a) isometric view from southeast direction; (b) typical plan, all dimensions in millimeters; (c) in-plane walls with boundary elements configuration

Table 1. Summary of Material Properties within Building III and Building IV

Material	Wall properties (MPa)	Building III	Building IV
Masonry	f'_m	19	17
	E_m	12,600	12,100
	G_m	5,050	4,850
Reinforcement	f_{yv}	500	450
	E_s	200,000	200,000

drift, Δ_u , after which the wall begins to lose lateral load capacity (Point C); the parameter e to represent the maximum drift, Δ_r , up to failure at Point E; and the parameter c to represent the residual strength corresponding to Points D and E. Although ASCE/SEI 41-13 (ASCE/SEI 2014) provides specific values for

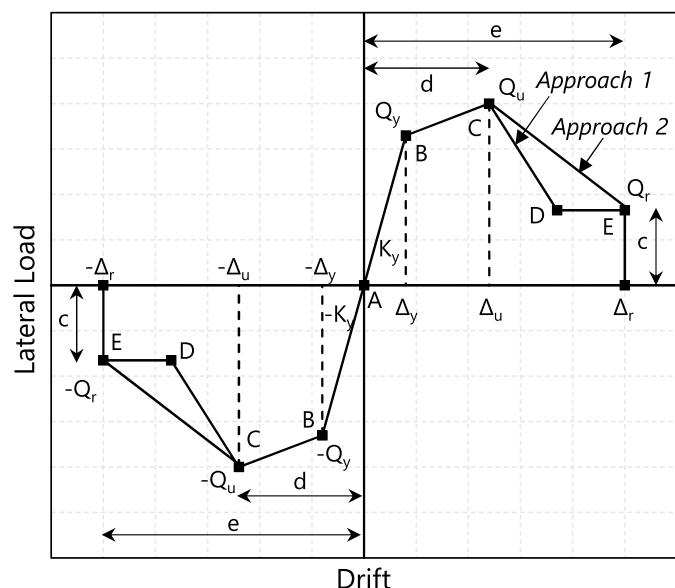


Fig. 3. Simplified load-drift relationship of reinforced masonry shear walls using ASCE/SEI 41-13 approaches

these parameters for RMSWs, thus defining Points B, C, and E, no parameters are given to define Point D in Approach 1. In addition, the steep transition between Points C and D may cause convergence problems in nonlinear analysis and may also not represent the actual response of RMSWs (ATC 2010). As such, ASCE/SEI 41-13 (ASCE/SEI 2014) proposes Approach 2 through the use of a modified slope from Point C to Point E, as shown in Fig. 3, to represent the postpeak response.

Current ASCE/SEI 41-13 Backbone Model Parameters

There are three key points needed to determine the individual wall response, as shown in Fig. 3. For the yield strength, Q_y , a linear strain profile is used to calculate the yield moment, M_y , with a yield strain of the outermost steel reinforcement set to 0.0025. To calculate the wall ultimate strength, Q_u , based on the ultimate moment, M_u , the ultimate masonry strain is taken as 0.0025, as specified by the TMS 402-13/ACI 530-13/ASCE 5-13 (MSJC 2013). Finally, the residual strength, Q_r , is calculated by multiplying Q_u by the parameter c specified in ASCE/SEI 41-13 (ASCE/SEI 2014), as discussed in the previous section. For all three strength calculation cases, a bending moment diagram must be assumed to relate the moment to the lateral load. To account for the effect of slab coupling, this diagram was selected based on the results of both experimental programs (i.e., Building III and Building IV), which

showed the significant effect of the diaphragm coupling in terms of changing the system-level response of the RMSWs aligned along the main direction of loading. More specifically, the orthogonal walls resulted in a coupling moment at the top level, M_{top} , due to the effect of tension force developed at yielding of the reinforcement, T_o , in each pair of the orthogonal walls balanced by an equal compression force, P_o , in the other pair of the orthogonal walls. The T_o in each orthogonal wall pair is equal to 180 and 162 kN for Buildings III and IV, respectively. As such, the coupling moment, M_{top} , is equal to the tension or compression force in one pair of the orthogonal walls multiplied by the distance between the orthogonal wall pairs. This coupling moment is then distributed to the other walls according to their effective moment of inertia, I_e . The coupling at the first level was much less significant. These calculations are supported by the numerical model developed by Ezzeldin et al. (2017a), which indicates that the diaphragm coupling influenced the system-level behavior of Building IV by restraining the in-plane rotations of the walls at the top slab level with minor coupling at the first floor slab level, as shown in Figs. 4(a and b). However, the diaphragm coupling decreases gradually at higher drift levels because of the cracks that develop within the diaphragm, until the walls of Building IV respond almost as cantilevers at large drifts, as shown in Fig. 4(c). Consistent observations were reported for Building III by Ashour and El-Dakhkhni (2016). As a simplification of this behavior, the walls aligned along the loading direction in both buildings are assumed to have linear variation of moment over the height from M_y or M_u at the base to M_{top} at the top, until reaching the ultimate point (i.e., Point C), as shown in Figs. 5(a and b). At the strength degradation point (i.e., Point E), the walls are assumed to be unrestrained by the slab, as shown in Fig. 5(c). Based on these assumptions, Eqs. (1a)–(1c) were used to calculate Q_y , Q_u , and Q_r , respectively, while the bending moments (i.e., M_y , M_u , M_{top} , and cM_u) used in these equations are given in Table 2. The elastic stiffness, K_y , and the yield drift, Δ_y , were calculated using Eqs. (2) and (3), respectively, according to Paulay and Priestley (1992)

$$Q_y = \frac{M_{top} + M_y}{h} \quad (1a)$$

$$Q_u = \frac{M_{top} + M_u}{h} \quad (1b)$$

$$Q_r = \frac{cM_u}{h} \quad (1c)$$

$$K_y = \frac{1}{\frac{h^3}{12E_m I_e} + \frac{1.2h}{G_m A_e}} \quad (2)$$

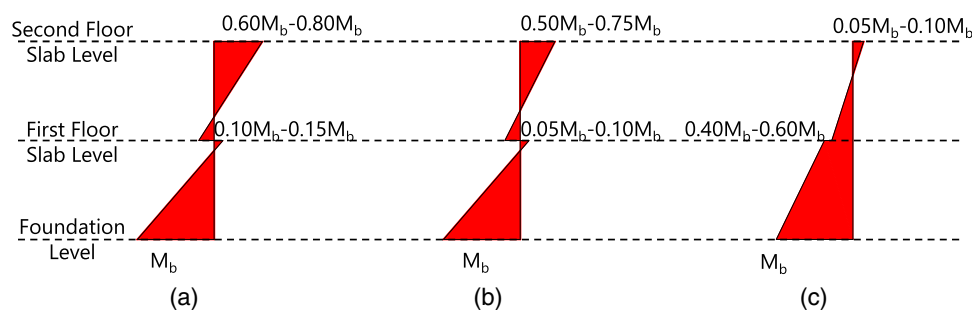


Fig. 4. Bending moments along the wall height of Building IV based on the numerical model developed by Ezzeldin et al. (2016): (a) at drift = 0.25%; (b) at drift = 0.90%; (c) at drift = 2.00%

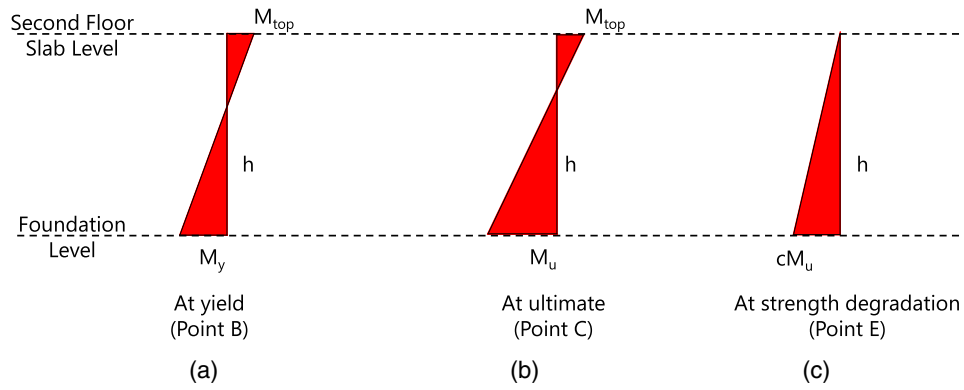


Fig. 5. Assumed bending moments along the wall height: (a) yield point; (b) ultimate point; (c) strength degradation point

Table 2. Summary of Bending Moments along the Wall Height within Building III and Building IV

Building	Wall	Bending moment along the wall height (kN · m)					
		At yield (Point B)		At ultimate (Point C)		At strength degradation (Point E)	
		M_y	M_{top}	M_u	M_{top}	cM_u	
Building III	W1 _{III} and W2 _{III}	21	8	31	8	19	
	W5 _{III}	122	128	184	128	110	
	W8 _{III}	189	224	263	224	158	
Building IV	W1 _{IV} and W2 _{IV}	23	12	29	12	22	
	W5 _{IV}	153	150	178	150	134	
	W8 _{IV}	193	150	239	150	179	

$$\Delta_y = \frac{Q_y}{K_y} \quad (3)$$

where h = wall height; the parameter c is determined as discussed earlier; E_m = masonry Young's modulus; G_m = masonry shear modulus; I_e = wall effective moment of inertia; and A_e = effective masonry wall cross-sectional area. Eq. (4) was used to calculate I_e and A_e , according to Paulay and Priestley (1992), where α is a stiffness reduction factor, I_g is the wall gross moment of inertia, A_g is the gross masonry wall cross-sectional area, f_{yv} is the yield strength of the vertical bars, f'_m is the masonry compressive strength, and P is the axial load on the wall. These material characteristics are given in Table 1 for Buildings III and IV

$$I_e = \alpha I_g \quad A_e = \alpha A_g \quad \alpha = \left(\frac{100}{f_{yv}} + \frac{P}{f'_m A_g} \right) \quad (4)$$

Finally, while ASCE/SEI 41-13 (ASCE/SEI 2014) provides the c , d , and e parameters to determine Δ_u and Δ_r , respectively, of RMSWs with rectangular cross sections, no corresponding parameters are given for RMSWs with boundary elements. As such, the parameters for RMSWs with the same properties but with rectangular cross sections, given in Table 3, were used to predict the response of the individual shear walls in Buildings III and IV.

Assessment of Current Modeling Approaches

The experimental results of Building III and Building IV were used to assess the current RMSW backbone models in ASCE/SEI 41-13 (ASCE/SEI 2014) using both Approaches 1 and 2, as discussed

Table 3. Summary of Model Parameters Assigned to RMSWs within Building III and Building IV (Data from ASCE/SEI 2014, © ASCE)

Wall	Model parameters		
	c (%)	d (% drift)	e (% drift)
W1 _{III/IV} and W2 _{III/IV}	67	0.66	1.32
W5 _{III/IV}	67	0.40	0.80
W8 _{III/IV}	70	0.30	0.60

earlier. The system-level response of Building III and Building IV was calculated through the superposition of the backbone model of the RMSWs aligned along the primary direction of loading at each displacement demand, while the resistance of the orthogonal walls was not considered because of their negligible strength in their out-of-plane direction (Heerema et al. 2015; Ashour and El-Dakhkhni 2016). The twist effects within both buildings were implemented in the superposition procedure using the displacement of each wall aligned along the primary direction of loading obtained from the experimental results, and subsequently calculating the corresponding wall resistance using the individual wall backbone model. Finally, the lateral strengths of Building III, Q_{III} , and Building IV, Q_{IV} , were calculated at each displacement demand using Eqs. (5) and (6), respectively

$$Q_{III} = 2 \times Q_{W1_{III}} + Q_{W5_{III}} + Q_{W8_{III}} \quad (5)$$

$$Q_{IV} = 2 \times Q_{W1_{IV}} + Q_{W5_{IV}} + Q_{W8_{IV}} \quad (6)$$

Figs. 6(a and b) compare the experimental lateral load versus the displacement at the building roof C_M to the model predictions for Buildings III and IV, respectively, using Approaches 1 and 2 shown in Fig. 3. In addition, Table 4 summarizes the error of the model predictions for the same buildings. In calculating these values, the drift at Point D in Approach 1 was assumed to be equal to the average drift of Points C and E, which resulted in a small slope to the segment between Points C and D in Fig. 3, as suggested by ATC (2010). As shown in Table 4, the model predicts the yield strength, Q_y (i.e., at 0.25% drift) of Buildings III and IV to within a maximum error of 20 and 15%, respectively. In addition, the ultimate strength, Q_u , is captured closely, with Fig. 6 showing a maximum error of less than 20 and 11% relative to the experimental results of Buildings III and IV, respectively. These results confirm the importance of including the out-of-plane stiffness of the floor diaphragms, as neglecting this stiffness by assuming cantilever walls would have underestimated the strength of Buildings III and IV by approximately 50% (Ezzeldin et al. 2017a). However, the

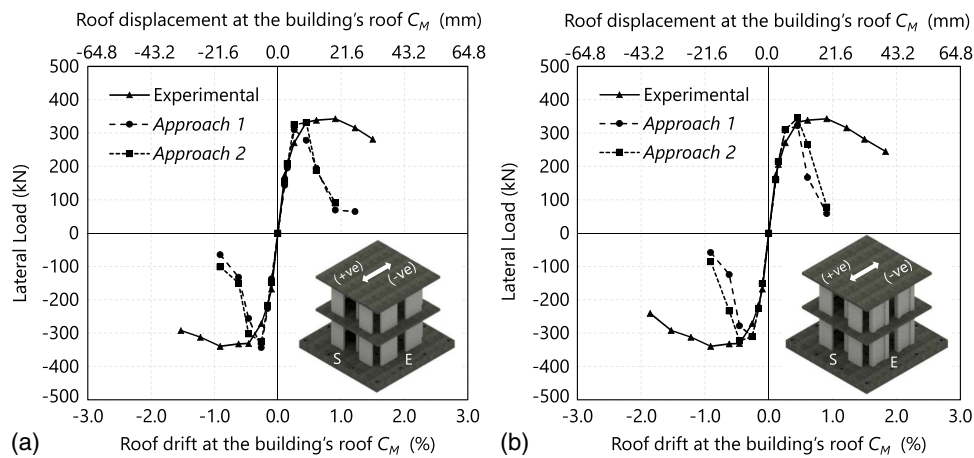


Fig. 6. Experimental and analytical envelopes based on ASCE/SEI 41-13 approaches: (a) Building III (data from Ashour et al. 2016, © ASCE); (b) Building IV (data from Ezzeldin et al. 2017b, © ASCE)

Table 4. Error for the Predicted Values Using the Current Backbone Models in ASCE/SEI 41-13 versus the Experimental Data at Different Drift Levels

Building	Approach	Error													
		Negative loading direction (drift)							Positive loading direction (drift)						
		-1.80 (%)	-1.50 (%)	-1.20 (%)	-0.90 (%)	-0.60 (%)	-0.40 (%)	-0.25 (%)	0.25 (%)	0.40 (%)	0.60 (%)	0.90 (%)	1.20 (%)	1.50 (%)	1.80 (%)
Building III ^a	1	N/A	—	—	-83	-64	-28	20	8	-21	-47	-83	-82	—	N/A
	2	N/A	—	—	-71	-55	-10	18	20	-2	-45	-74	—	—	N/A
Building IV ^b	1	—	—	—	-83	-63	-15	15	15	3	-51	-84	—	—	—
	2	—	—	—	-75	-30	-3	15	15	5	-21	-78	—	—	—

Note: N/A = experimental data not available. Entries with — denote model predicting zero strength.

^aBased on data from Ashour et al. (2016).

^bBased on data from Ezzeldin et al. (2017b).

model fails to predict the postyield branch of the experimental results of both buildings. As shown in Table 4, an error of up to 84% is reported for both predicted postyield load-displacement relationships. This is primarily attributed to the very conservative values of the parameters c , d , and e in ASCE/SEI 41-13 (ASCE/SEI 2014) for RMSWs. As such, the following section outlines the development of an analytical model that is capable of more accurately predicting the backbone of the load-displacement relationships of Buildings III and IV up to and following the ultimate strength point.

Proposed RMSW Building Backbone Model for ASCE/SEI 41

Model Development

The proposed backbone model defines the RMSW deformations in terms of elastic and plastic rotations using the generalized backbone curve relationship shown in Fig. 7. The elastic segment up to Point B is defined by the elastic rotation, θ_y . The plastic rotation up to loss of the lateral load capacity at Point C, θ_u , is represented by the parameter a , while the parameter b represents the plastic rotation up to failure at Point E, θ_r . The parameter c is also used to define the residual moment of Point D, M_r . Although ASCE/SEI 41-13 (ASCE/SEI 2014) provides these parameters (i.e., a , b , and c) for reinforced concrete shear walls (RCSWs), no corresponding values are currently given for RMSWs. As such, the parameters specified for RCSWs, given in Table 5, were used to predict the response of the individual shear walls in Buildings III and IV. This

approach was considered acceptable during the model development because fully grouted structural RMSW construction is very similar to structural RCSW construction in terms of the material behavior and the analysis of displacements (Shedid et al. 2010; Banting and El-Dakhakhni 2014). In addition, several experimental studies have

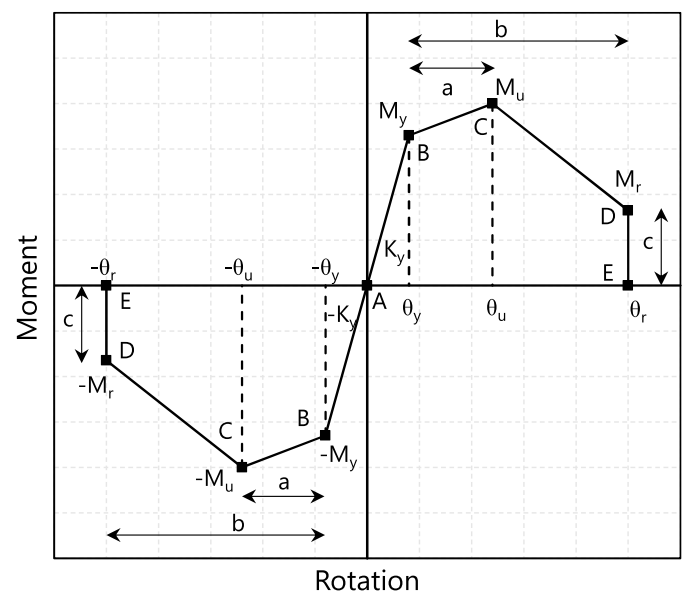


Fig. 7. Proposed simplified moment-rotation relationship for reinforced masonry shear walls without and with boundary elements

Table 5. Summary of Model Parameters Assigned to the Proposed Model of RMSWs within Building III and Building IV (Data from ASCE/SEI 2014, © ASCE)

Building	Model parameters		
	a (rad)	b (rad)	c (%)
Building III	0.006	0.015	60
Building IV	0.010	0.020	75

shown that high levels of ductility and small strength degradation, similar to those of RCSWs, can be achieved with RMSWs (Shing et al. 1990; Seible et al. 1993; Eikanas 2003; Shedid et al. 2008). ASCE/SEI 41-13 (ASCE/SEI 2014) also considers the enhanced lateral deformation capacity of RCSWs with confined boundary elements by assigning higher distinctive values for the above parameters (i.e., a , b , and c) to those walls than the corresponding values assigned to traditional shear walls with rectangular cross sections, so the same enhanced parameters, given in Table 5, were used for Building IV.

Fig. 8 summarizes how to evaluate the key points to build the proposed model. Point A represents the unloaded condition, while Point B defines the effective yield point through Q_y and Δ_y , which

were given previously in Eqs. (1a) and (3), respectively. Point C represents the ultimate strength point, where Q_u and Δ_u can be calculated from Eqs. (1b) and (7a), respectively

$$\Delta_u = \Delta_y + a(h - l_p) \quad (7a)$$

In Eq. (7a), l_p is the plastic hinge length of the wall, assumed to be 50% of the wall flexural depth but less than the wall height and less than 50% of the wall length, according to ASCE/SEI 41-13 (ASCE/SEI 2014). Point D is a point defining the residual strength through Q_r and Δ_r , which can be determined from Eqs. (1c) and (7b), respectively

$$\Delta_r = \Delta_y + b(h - l_p) \quad (7b)$$

At deformation levels beyond Point D, the wall strength is assumed to drop to zero, as represented by Point E. The load-displacement relationships of the individual walls aligned along the primary direction of loading of Buildings III and IV, shown in Figs. 9(a and b), respectively, were predicted following Fig. 8. As Figs. 9(a and b) show, Δ_u and Δ_r of the walls in Building IV increase by an average of 35 and 30%, respectively, relative to their corresponding walls in Building III. This indicates the importance

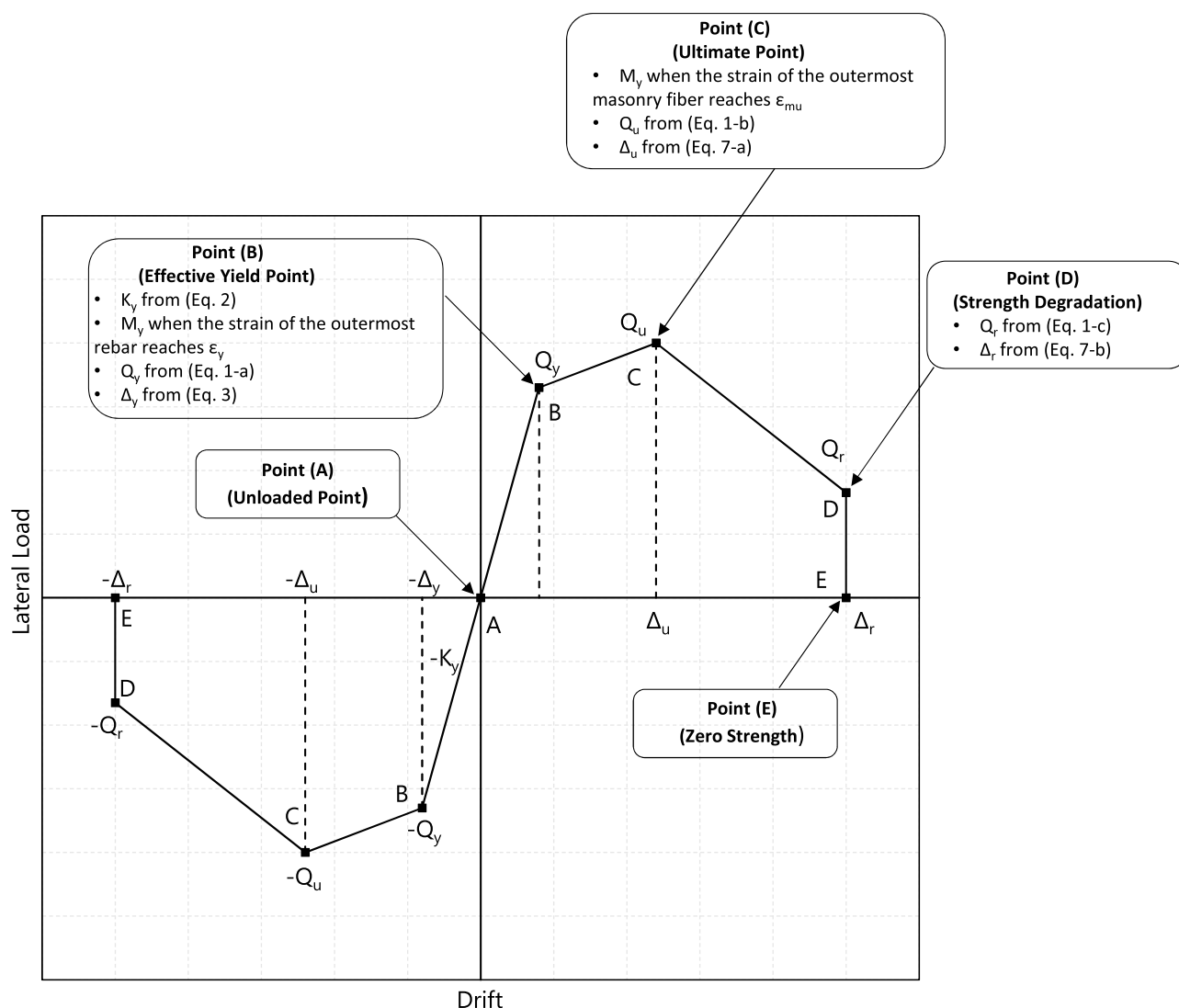


Fig. 8. Proposed simplified load-drift relationship for reinforced masonry shear walls without and with boundary elements

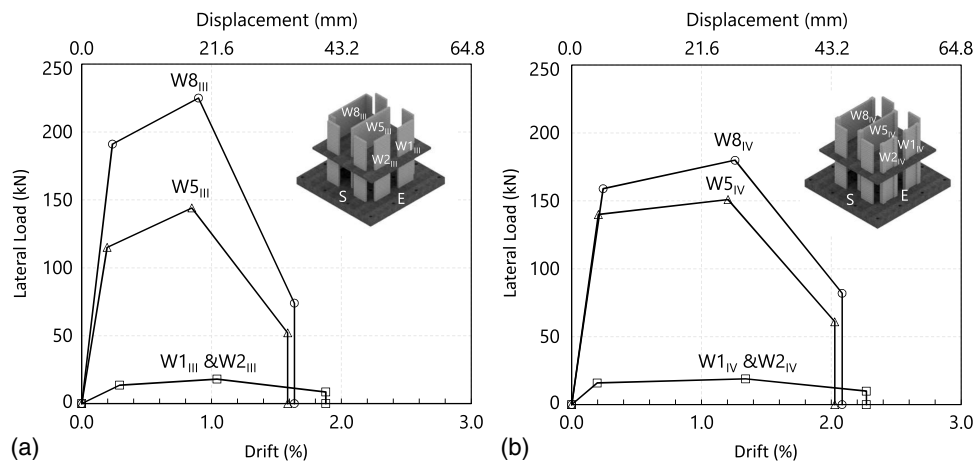


Fig. 9. Load-drift relationship of walls aligned along the loading direction: (a) Building III (data from Ashour et al. 2016, © ASCE); (b) Building IV (data from Ezzeldin et al. 2017b, © ASCE)

of including the confinement effect of the boundary elements when estimating the RMSW performance. In addition, Figs. 9(a and b) show that the walls within each building do not all respond plastically simultaneously. Therefore, adding the strengths of all walls, by assuming that all walls simultaneously reach their ultimate capacities and have adequate ductility to sustain these capacities (ASCE/SEI 2014), would overestimate the overall building resistance. This confirms the importance of system-level studies used in this paper to validate the developed model.

Comparison of Model Predictions with System-Level Experimental Responses

The system-level response of Buildings III and IV was evaluated through the superposition of the backbone models of all RMSWs aligned along the primary direction of loading at each displacement demand level, considering building twist as discussed earlier. Fig. 10(a) compares the prediction of the proposed model with the experimental results for Building III, and Table 6 summarizes the percentage error of the model predictions relative to the experimental data of the same building. As Fig. 10(a) and Table 6 show, the lateral load of the building is predicted very closely for most of

the lateral drift levels, with a maximum error in the lateral load prediction of less than 9%. In addition, the model captures the yield strength, Q_y , to within 14% error. The proposed model results are compared also with the experimental results of Building IV in Fig. 10(b) and Table 6. Relative to the experimental results, the maximum error in the lateral load is less than 10%. In addition, the maximum difference between analytical and experimental yield strength, Q_y , is less than 13%.

These results confirm the effectiveness of the proposed parameters a , b , and c for predicting the response of Buildings III and IV. Figs. 10(a and b) show that the model is able to simulate most relevant characteristics of the response at all considered drift levels, including the postultimate range (i.e., strength degradation), whereas the current parameters assigned to RMSWs in ASCE/SEI 41-13 (ASCE/SEI 2014) significantly underestimated the postyield branch of the experimental results, as previously shown in Fig. 6. This indicates that the parameters that ASCE/SEI 41-13 (ASCE/SEI 2014) assigns to RMSWs with rectangular cross sections (c , d , and e) may be unnecessarily conservative and may require revision. This conservatism was based on the limited number of experimental studies at the time when FEMA 356 (FEMA 2000), *Prestandard and commentary for the seismic rehabilitation of*

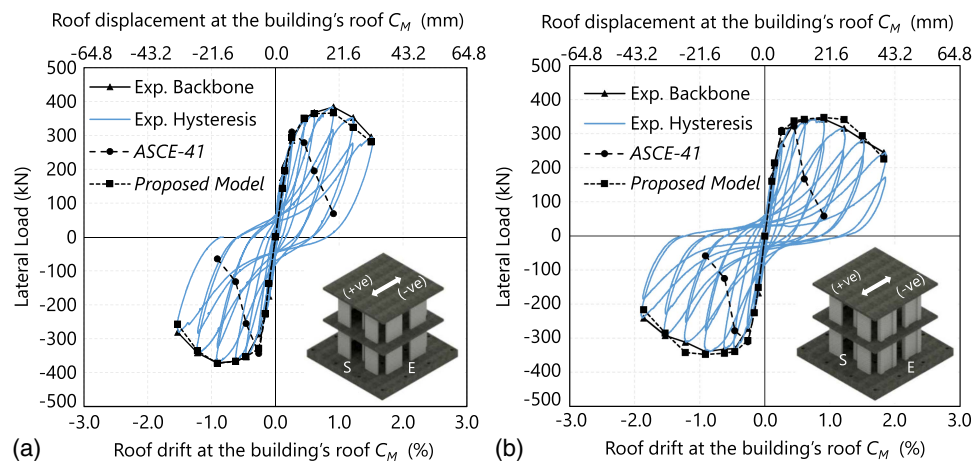


Fig. 10. Experimental (backbone and hysteresis) and analytical envelopes based on ASCE/SEI 41-13 using Approach 1 and the proposed modeling approach: (a) Building III (data from Ashour et al. 2016, © ASCE); (b) Building IV (data from Ezzeldin et al. 2017b, © ASCE)

Table 6. Error for the Predicted Values Using the Proposed Backbone Model in ASCE/SEI-41 versus the Experimental Data at Each Drift Level

Building	Error													
	Negative loading direction (drift)							Positive loading direction (drift)						
	-1.80 (%)	-1.50 (%)	-1.20 (%)	-0.90 (%)	-0.60 (%)	-0.40 (%)	-0.25 (%)	0.25 (%)	0.40 (%)	0.60 (%)	0.90 (%)	1.20 (%)	1.50 (%)	1.80 (%)
Building III ^a	N/A	-9	-2	1	1	-1	-14	3	1	-1	-5	-9	-5	N/A
Building IV ^b	-10	-2	10	3	4	3	13	13	2	1	2	9	5	-8

Note: N/A = experimental data not available.

^aBased on data from Ashour et al. (2016).

^bBased on data from Ezzeldin et al. (2017b).

buildings, was originally developed. In addition, distinctive corresponding values are needed for RMSWs with boundary elements to consider the enhanced lateral deformation capacity achieved when they are adopted (Shedid et al. 2010; Banting and El-Dakhkhni 2012, 2014; Cyrier 2012; El Ezz et al. 2015; Ezzeldin et al. 2016; 2017b). These results suggest that the parameters currently given for RCSW in ASCE/SEI 41-13 (ASCE/SEI 2014) may be appropriate.

RMSW Building Hysteretic Model for ASCE/SEI 41

Model Development

The nonlinear dynamic procedure (NDP) evaluates the inelastic demands of a structure subjected to a suite of ground motion records based on nonlinear time history analysis (ASCE/SEI 2014; FEMA 2000). The NDP is considered a more refined procedure compared to NSP because it represents the demands the structure would experience during a specific seismic event (ASCE/SEI 2014), including the expected shifts in inertial load patterns as softening occurs within the structure. However, the NDP requires hysteretic models that are able to capture not only the initial stiffness, peak load, and strength deterioration, but also the stiffness degradation, hysteretic shape, and pinching behavior.

In this respect, a simplified numerical model is developed in this paper using OpenSees and validated against the experimental results of Buildings III and IV. The developed numerical model adopts a concentrated plasticity approach, where elastic

beam-column elements are used to model the walls of both buildings, with the wall inelastic behavior accounted for through a zero-length inelastic rotational spring at the base of each wall, as shown in Fig. 11(a). These springs follow a bilinear hysteretic response based on the modified Ibarra-Medina-Krawinkler deterioration response model with pinching hysteretic response (Ibarra et al. 2005, ModIMKPinching material in OpenSees). The model is represented by a moment-rotation relationship, as shown in Fig. 11(b), that depends on the yield moment, M_y ; the ultimate moment, M_u ; the residual moment, M_r ; the rotational stiffness, K_θ ; the preultimate plastic rotation, θ_p ; the postultimate plastic rotation, θ_{pc} ; and other parameters that define strength deterioration and pinching behavior. The parameters M_y , M_u , and M_r were defined earlier, while K_θ , θ_p , and θ_{pc} are calculated from Eqs. (8), (9a), and (9b), respectively, in terms of the previously defined parameters I_e , h , θ_y , θ_u , and θ_r

K_theta = ((n + 1) * 6 * E * I_e) / h

theta_p = theta_u - theta_y

theta_pc = theta_r - theta_u

In Eq. (8) a stiffness modifier, n , of value 10 is used in calculating the rotational stiffness, K_θ , since the wall is modeled as a rotational spring connected in series with an elastic beam-column element, as shown in Fig. 11(b) (Ibarra and Krawinkler 2005). Subsequently, the stiffness of these components is modified so that

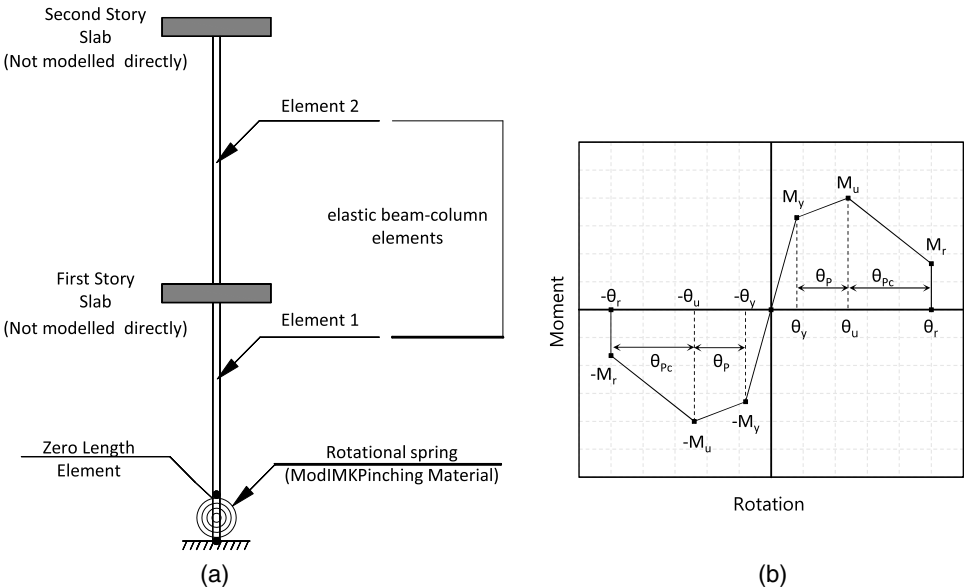


Fig. 11. Schematic diagram of the model

their equivalent stiffness, K_w , is equal to the stiffness of the actual wall. For this reason and also to avoid any numerical problems, the rotational spring stiffness, K_θ , and the elastic element stiffness, K_e , are multiplied by modification factors of $(n + 1)$ and $(n + 1/n)$, respectively, as suggested by Ibarra and Krawinkler (2005), and wall equivalent stiffness, K_w , is then calculated as

$$K_w = \frac{K_\theta K_e}{K_\theta + K_e} \quad (10)$$

The strength deterioration and pinching behavior parameters were defined using the values suggested by Lignos and Krawinkler (2013) based on a database of 200 RC components with different configurations. The model accounts for the boundary conditions through the calculation of K_θ , where the RMSWs are considered fixed at the foundation and partially fixed at the roof levels [from Eq. (8)]. Therefore, the RC floor slabs of Buildings III and IV were modeled considering a diaphragm possessing no out-of-plane stiffness, while still being stiff in the in-plane direction.

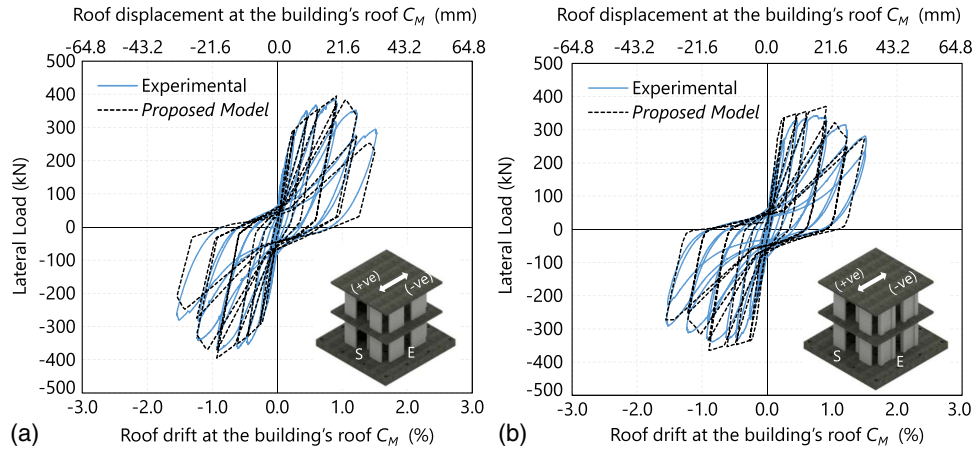


Fig. 12. Experimental and numerical hysteresis loops: (a) Building III (data from Ashour et al. 2016, © ASCE); (b) Building IV (data from Ezzeldin et al. 2017b, © ASCE)

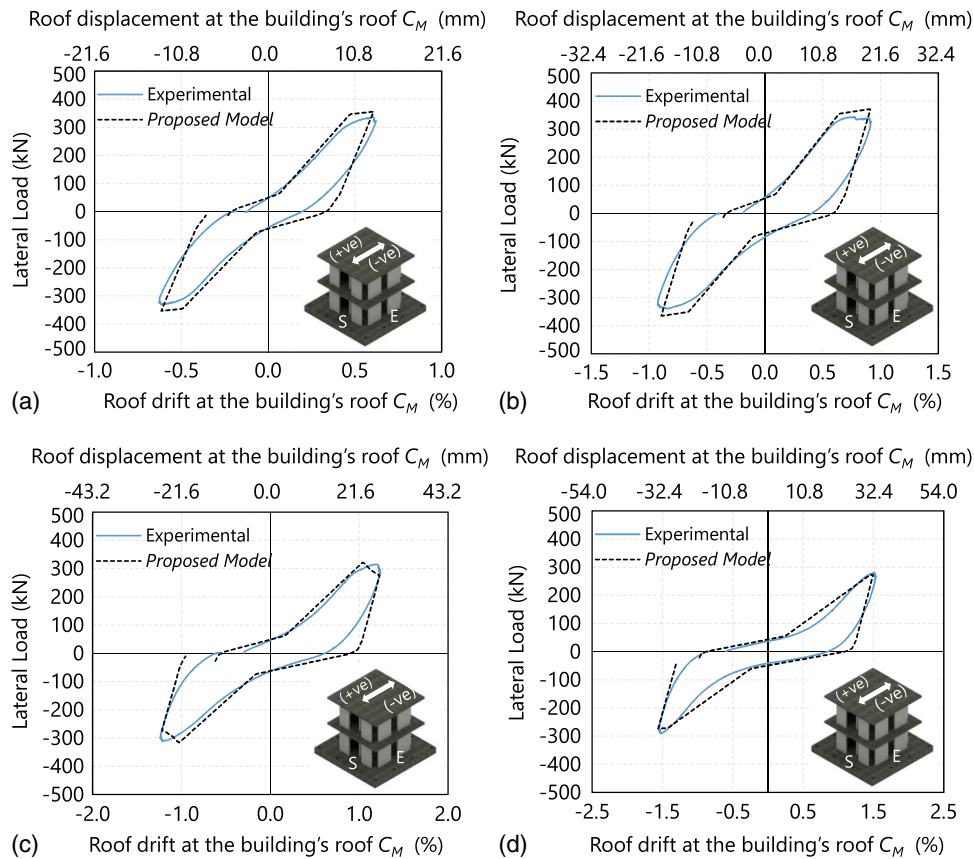


Fig. 13. Detailed experimental and numerical hysteresis loops of Building IV (data from Ezzeldin et al. 2017b, © ASCE): (a) at drift = 0.60%; (b) at drift = 0.90%; (c) at drift = 1.20%; (d) at drift = 1.50%

Model Validation

Fig. 12(a) compares the results of the numerical model with the corresponding experimental results for Building III tested by Ashour et al. (2016). The figure shows that the model is capable of simulating most relevant characteristics of the cyclic response at all tested drift levels. The drift ranges in Fig. 12 cover the entire load-displacement curve up to degradation to 80% of the ultimate strength. The lateral capacity of the building is predicted closely for most of the lateral drift levels, with a maximum deviation in the lateral load prediction of less than 16%. In addition, the increase of energy dissipation with loading is represented well by the hysteretic model, with a maximum deviation of 15% compared to the experimental results.

To verify the effectiveness of the developed model for buildings with boundary elements, the model results are compared with the experimental results from Building IV (Ezzeldin et al. 2017b) in Fig. 12(b). The individual experimental and numerical hysteresis loops for the same building, using the first cycle at each of the second floor drift levels, are shown in Fig. 13. Relative to the experimental results, the maximum error in the lateral load prediction is less than 10%. In addition, the model captures the energy dissipation with a maximum error of approximately 9%. Overall, the comparison between the experimental and numerical results shows that the proposed model, based on previous results for RCSWs, is capable of capturing the hysteretic response of RMSW buildings both with and without boundary elements.

Conclusions

The NSP and the NDP, specified in ASCE/SEI 41-13 (ASCE/SEI 2014), require nonlinear structural response models that are capable of predicting the inelastic behavior of buildings at different performance levels. The results demonstrated that existing recommendations for RMSWs may not adequately predict this behavior. As such, this study proposed alternative new backbone and hysteretic models that can be used in the NSP and the NDP, respectively, to simulate the nonlinear response of shear wall buildings with different configurations. Subsequently, these models were validated against the experimental results of Buildings III and IV reported by Ashour et al. (2016) and Ezzeldin et al. (2017b), respectively. The backbone model accurately captured the complete load-displacement relationships of both buildings, with maximum errors of 14%. In addition, a hysteretic model was developed using *OpenSees* to simulate the hysteretic response of RMSW buildings. The inelastic behavior of each wall in that model is represented by a zero-length inelastic rotational spring at the base of the wall. Finally, the results showed that the developed model satisfies the ASCE/SEI 41-13 (ASCE/SEI 2014) requirements in terms of simulating the initial stiffness, peak load, stiffness degradation, strength deterioration, hysteretic shape, and pinching behavior at different drift levels.

In general, the results confirmed the importance of including out-of-plane stiffness of the floor diaphragms to estimate the overall building response. In addition, the results showed that the current parameters assigned to RMSWs in ASCE/SEI 41-13 need to be revised, because the models developed based on those parameters failed to capture the postyield branch of the experimental results. Moreover, ASCE/SEI 41-13 (ASCE/SEI 2014) provides parameters with numerical values given only for RMSWs with rectangular cross sections. This study showed that distinctive values for such parameters should be provided for RMSWs with boundary elements, so as to consider the enhanced lateral deformation capacity achieved when such seismic-force-resisting systems are adopted.

These values may be based on what is currently specified for concrete shear walls.

Finally, the analyses in this paper were based on the results of two two-story RMSW buildings with specific design characteristics (i.e., material properties) and configurations (i.e., geometrical properties), with one of the buildings constructed using walls with rectangular cross sections and the other using walls with boundary elements. As such, the experimental results of more RMSW buildings with different numbers of stories and wall configurations are expected to further improve the predictability of the developed models presented in this study, and subsequently facilitate the development of prescriptive design requirements for such SFRS.

Acknowledgments

The financial support for this project was provided through the Natural Sciences and Engineering Research Council of Canada (NSERC) and the Canada Masonry Design Centre (CMDCC). Additional support was also provided by the McMaster University Centre for Effective Design of Structures, funded through the Ontario Research and Development Challenge Fund of the Ministry of Research and Innovation (MRI). The provision of the scaled blocks through a grant from the Canadian Concrete Masonry Producers Association (CCMPA) is gratefully acknowledged.

Notation

The following symbols are used in this paper:

- A_e = effective cross section area;
- A_g = gross cross section area;
- a = plastic rotation up to loss of the wall lateral load capacity;
- b = plastic rotation up to wall failure;
- C_M = building floor center of mass;
- C_R = building center of rigidity;
- c = residual moment/strength ratio;
- d = parameter to represent the ultimate drift;
- E_m = Masonry Young's modulus;
- e = parameter to represent the maximum drift;
- f'_m = masonry compressive strength;
- f_{yv} = vertical reinforcement yield strength;
- G_m = masonry shear modulus;
- h = wall height;
- I_e = effective moment of inertia;
- I_g = gross moment of inertia;
- K_e = elastic element stiffness;
- K_w = wall equivalent stiffness;
- K_y = elastic stiffness;
- K_θ = spring rotational stiffness;
- l_p = plastic hinge length of the wall;
- M_r = residual moment;
- M_{top} = top coupling moment;
- M_u = ultimate moment;
- M_y = yield moment;
- P = wall axial load;
- P_o = orthogonal walls compression force;
- Q_r = residual strength;
- Q_u = ultimate strength;
- Q_y = yield strength;
- Q_{III} = lateral strength of Building III;
- Q_{IV} = lateral strength of Building IV;
- T_o = orthogonal walls tension force;

α = reduction factor;
 Δ_r = maximum drift ratio;
 Δ_u = ultimate drift ratio;
 Δ_y = yield drift ratio;
 θ_p = preultimate rotation;
 θ_{pc} = postultimate rotation;
 θ_r = maximum rotation capacity;
 θ_u = ultimate rotation; and
 θ_y = yield rotation.

References

- Abdellatef, M. (2011). "The development of a simplified modelling technique for the finite element analysis of reinforced masonry shear walls." M.Sc. thesis, Dept. of Civil and Environmental Engineering, Washington State Univ., Pullman, WA.
- Andreini, M., De Falco, A., Giresini, L., and Sassu, M. (2014). "Mechanical characterization of masonry walls with chaotic texture: Procedures and results of in-situ tests." *Int. J. Archit. Herit.*, 8(3), 376–407.
- ASCE/SEI (Structural Engineering Institute). (2014). "Seismic evaluation and retrofit of existing buildings." *ASCE/SEI 41-13*, Reston, VA.
- Ashour, A., and El-Dakhkhni, W. (2016). "Influence of floor diaphragm-wall coupling on the system-level seismic performance of an asymmetrical reinforced concrete block building." *J. Struct. Eng.*, 10.1061/(ASCE)ST.1943-541X.0001540, 04016071.
- Ashour, A., El-Dakhkhni, W., and Shedid, M. (2016). "Experimental evaluation of the system-level seismic performance and robustness of an asymmetrical reinforced concrete block building." *J. Struct. Eng.*, 10.1061/(ASCE)ST.1943-541X.0001529, 04016072.
- ATC (Applied Technology Council). (2010). "Modeling and acceptance criteria for seismic design and analysis of tall buildings." *PEER/ATC Rep. No. 72-1*, Redwood City, CA.
- Banting, B., and El-Dakhkhni, W. (2012). "Force-and displacement-based seismic performance parameters for reinforced masonry structural walls with boundary elements." *J. Struct. Eng.*, 10.1061/(ASCE)ST.1943-541X.0000572, 1477–1491.
- Banting, B., and El-Dakhkhni, W. (2014). "Seismic performance quantification of reinforced masonry structural walls with boundary elements." *J. Struct. Eng.*, 10.1061/(ASCE)ST.1943-541X.0000895, 04014001.
- Cho, J. Y., and Pincheira, J. A. (2006). "Inelastic analysis of reinforced concrete columns with short lap splices subjected to reversed cyclic loads." *ACI Struct. J.*, 103(2), 280–290.
- Clough, R. W. (1966). *Effect of stiffness degradation on earthquake ductility requirements*, Univ. of California, Berkeley, CA.
- Cosenza, E., De Cicco, F., and Protà, A. (2010). "Discussion of 'Nonlinear uniaxial material model for reinforcing steel bars' by Sashi K. Kunnath, Yeong Ae Heo, and Jon F. Mohle." *J. Struct. Eng.*, 10.1061/(ASCE)ST.1943-541X.0000119, 917–918.
- CSA (Canadian Standards Association). (2014). "Design of masonry structures." *CSA S304-14*, Mississauga, Canada.
- Cyrier, W. B. (2012). "Performance of concrete masonry shear walls with integral confined concrete boundary elements." Ph.D. dissertation, Washington State Univ., Pullman, WA.
- De la Llera, J. C. L., and Chopra, A. K. (1995). "A simplified model for analysis and design of asymmetric-plan buildings." *Earthquake Eng. Struct. Dyn.*, 24(4), 573–594.
- Dides, M. A., and De la Llera, J. C. (2005). "A comparative study of concentrated plasticity models in dynamic analysis of building structures." *Earthquake Eng. Struct. Dyn.*, 34(8), 1005–1026.
- Dolšek, M., and Fajfar, P. (2008). "The effect of masonry infills on the seismic response of a four-storey reinforced concrete frame—A deterministic assessment." *Eng. Struct.*, 30(7), 1991–2001.
- Dymiotis, C., Kappos, A. J., and Chryssanthopoulos, M. K. (2001). "Seismic reliability of masonry-infilled RC frames." *J. Struct. Eng.*, 10.1061/(ASCE)0733-9445(2001)127:3(296), 296–305.
- Eikanas, I. (2003). "Behaviour of concrete masonry shear walls with varying aspect ratio and flexural reinforcement." M.S. thesis, Washington State Univ., Pullman, WA.
- El Ezz, A. A., Seif Eldin, H. M., and Galal, K. (2015). "Influence of confinement reinforcement on the compression stress-strain of grouted reinforced concrete block masonry boundary elements." *Structures*, 2, 32–43.
- Ezzeldin, M., El-Dakhkhni, W., and Wiebe, L. (2017b). "Experimental assessment of the system-level seismic performance of an asymmetrical reinforced concrete block-wall building with boundary elements." *J. Struct. Eng.*, 10.1061/(ASCE)ST.1943-541X.0001790, 04017063.
- Ezzeldin, M., Wiebe, L., and El-Dakhkhni, W. (2016). "Seismic collapse risk assessment of reinforced masonry walls with boundary elements using the FEMA P695 methodology." *J. Struct. Eng.*, 10.1061/(ASCE)ST.1943-541X.0001579, 04016108.
- Ezzeldin, M., Wiebe, L., and El-Dakhkhni, W. (2017a). "System-level seismic risk assessment methodology: Application to reinforced masonry buildings with boundary elements." *J. Struct. Eng.*, 10.1061/(ASCE)ST.1943-541X.0001815, 04017084.
- FEMA. (2000). "Prestandard and commentary for the seismic rehabilitation of buildings." *FEMA 356*, Washington, DC.
- FEMA. (2005). "Improvement of nonlinear static seismic analysis procedures." *FEMA 440*, Washington, DC.
- FEMA. (2009). "Quantification of building seismic performance factors." *FEMA P695*, Washington, DC.
- FEMA. (2012). "Seismic performance assessment of buildings." *FEMA P58-1*, Washington, DC.
- Giambanco, G., Rizzo, S., and Spallino, R. (2001). "Numerical analysis of masonry structures via interface models." *Comput. Meth. Appl. Mech. Eng.*, 190(49), 6493–6511.
- Giberson, M. (1967). "The response of nonlinear multi-story structures subjected to earthquake excitation." Ph.D. thesis, California Institute of Technology, Pasadena, CA.
- Guinea, G. V., Hussein, G., Elices, M., and Planas, J. (2000). "Micromechanical modeling of brick-masonry fracture." *Cem. Concr. Res.*, 30(5), 731–737.
- Heerema, P., Shedid, M., Konstantinidis, D., and El-Dakhkhni, W. (2015). "System-level seismic performance assessment of an asymmetrical reinforced concrete block shear wall building." *J. Struct. Eng.*, 10.1061/(ASCE)ST.1943-541X.0001298, 04015047.
- Ibarra, L. F., and Krawinkler, H. (2005). "Global collapse of frame structures under seismic excitations." Pacific Earthquake Engineering Research Center, Berkeley, CA.
- Ibarra, L. F., Medina, R. A., and Krawinkler, H. (2005). "Hysteretic models that incorporate strength and stiffness deterioration." *Earthquake Eng. Struct. Dyn.*, 34(12), 1489–1511.
- Karapitta, L., Mouzakis, H., and Carydis, P. (2011). "Explicit finite-element analysis for the in-plane cyclic behavior of unreinforced masonry structures." *Earthquake Eng. Struct. Dyn.*, 40(2), 175–193.
- Kim, S. H., and Koutouros, I. (2016). "Constitutive model for reinforcing steel under cyclic loading." *J. Struct. Eng.*, 10.1061/(ASCE)ST.1943-541X.0001593, 04016133.
- Kunnath, S., Heo, Y., and Mohle, J. (2010). "Closure to 'Nonlinear uniaxial material model for reinforcing steel bars' by Sashi K. Kunnath, Yeong Ae Heo, and Jon F. Mohle." *J. Struct. Eng.*, 10.1061/(ASCE)ST.1943-541X.0000197, 918–920.
- Kunnath, S. K., Heo, Y., and Mohle, J. F. (2009). "Nonlinear uniaxial model for reinforcing steel bars." *J. Struct. Eng.*, 10.1061/(ASCE)0733-9445(2009)135:4(335), 335–343.
- Lai, S. S., Will, G. T., and Otani, S. (1984). "Model for inelastic biaxial bending of concrete members." *J. Struct. Eng.*, 10.1061/(ASCE)0733-9445(1984)110:11(2563), 2563–2584.
- Lignos, D. G., and Krawinkler, H. (2013). "Development and utilization of structural component databases for performance-based earthquake engineering." *J. Struct. Eng.*, 10.1061/(ASCE)ST.1943-541X.0000646, 1382–1394.
- Lourenço, P. B., and Rots, J. G. (1997). "Multisurface interface model for analysis of masonry structures." *J. Eng. Mech.*, 10.1061/(ASCE)0733-9399(1997)123:7(660), 660–668.

- Maekawa, K., Pinanmas, A., and Okamura, H. (2003). *Nonlinear mechanics of reinforced concrete*, Spon Press, New York.
- Marques, R., and Lourenço, P. B. (2014). "Unreinforced and confined masonry buildings in seismic regions: Validation of macro-element models and cost analysis." *Eng. Struct.*, 64, 52–67.
- Mojsilovic, N., and Marti, P. (1997). "Strength of masonry subjected to combined actions." *ACI Struct. J.*, 94(6), 633–642.
- Monti, G., and Spacone, E. (2000). "Reinforced concrete fiber beam element with bond-slip." *J. Struct. Eng.*, 10.1061/(ASCE)0733-9445(2000)126:6(654), 654–661.
- MSJC (Masonry Standards Joint Committee). (2013). "Building code requirements and specifications for masonry structures." *TMS 402-13/ACI 530-13/ASCE 5-13*, American Concrete Institute, Detroit.
- Murcia-Delso, J., and Benson Shing, P. (2014). "Bond-slip model for detailed finite-element analysis of reinforced concrete structures." *J. Struct. Eng.*, 10.1061/(ASCE)ST.1943-541X.0001070, 04014125.
- OpenSees [Computer software]. Univ. of California, Berkeley, CA.
- Paulay, T. (1997). "Seismic torsional effects on ductile structural wall systems." *J. Earthquake Eng.*, 1(4), 721–745.
- Paulay, T., and Priestley, M. (1992). *Seismic design of reinforced concrete and masonry buildings*, Wiley, New York.
- Priestley, N., Calvi, G., and Kowalsky, M. (2007). *Displacement-based seismic design of structures*, IUSS Press, Pavia, Italy.
- Salem, H. M., and Maekawa, K. (2004). "Pre- and post-yield finite element method simulation of bond of ribbed reinforcing bars." *J. Struct. Eng.*, 10.1061/(ASCE)0733-9445(2004)130:4(671), 671–680.
- Seible, F., Kürschbasche, A. G., and Kingsley, G. R. (1993). "Three-dimensional analysis model for complete masonry buildings." *Structural engineering in natural hazards mitigation*, ASCE, Reston, VA, 1185–1190.
- Shedid, M. T., Drysdale, R. G., and El-Dakhakhni, W. W. (2008). "Behavior of fully grouted reinforced concrete masonry shear walls failing in flexure: Experimental results." *J. Struct. Eng.*, 10.1061/(ASCE)0733-9445(2008)134:11(1754), 1754–1767.
- Shedid, M. T., El-Dakhakhni, W. W., and Drysdale, R. G. (2010). "Alternative strategies to enhance the seismic performance of reinforced concrete-block shear wall systems." *J. Struct. Eng.*, 10.1061/(ASCE)ST.1943-541X.0000164, 676–689.
- Shing, P. B., Schuller, M., and Hoskere, V. S. (1990). "In-plane resistance of reinforced masonry shear walls." *J. Struct. Eng.*, 10.1061/(ASCE)0733-9445(1990)116:3(619), 619–640.
- Siyam, M., El-Dakhakhni, W., Shedid, M., and Drysdale, R. (2015). "Seismic response evaluation of ductile reinforced concrete block structural walls. I: Experimental results and force-based design parameters." *J. Perform. Constr. Facil.*, 10.1061/(ASCE)CF.1943-5509.0000794, 04015066.
- Stavridis, A., et al. (2011). "Shake-table tests of a 3-story, full-scale masonry wall system." *Proc., ACI Masonry Seminar*, Masonry Society, Longmont, CO.
- Stavridis, A., and Shing, P. B. (2010). "Finite-element modeling of nonlinear behavior of masonry-infilled RC frames." *J. Struct. Eng.*, 10.1061/(ASCE)ST.1943-541X.116, 285–296.
- Takizawa, H. (1976). "Notes on some basic problems in inelastic analysis of planar RC structures." *Trans. Archit. Inst. Jpn.*, 240, 51–62.
- Taucer, F., Spacone, E., and Filippou, F. C. (1991). *A fiber beam-column element for seismic response analysis of reinforced concrete structures*, Vol. 91, Univ. of California, Berkeley, CA.
- Waugh, J., and Sritharan, S. (2010). "Lessons learned from seismic analysis of a seven-story concrete test building." *J. Earthquake Eng.*, 14(3), 448–469.